

Journal of Biomedical Optics

SPIEDigitalLibrary.org/jbo

Dynamic multicomponent engineered tissue reorganization and matrix deposition measured with an integrated nonlinear optical microscopy–optical coherence microscopy system

Yuqiang Bai
Po-Feng Lee
Holly C. Gibbs
Kayla J. Bayless
Alvin T. Yeh

Dynamic multicomponent engineered tissue reorganization and matrix deposition measured with an integrated nonlinear optical microscopy–optical coherence microscopy system

Yuqiang Bai,^a Po-Feng Lee,^a Holly C. Gibbs,^a Kayla J. Bayless,^b and Alvin T. Yeh^{a,*}

^aTexas A&M University, Department of Biomedical Engineering, 5045 Emerging Technologies Building, College Station, Texas 77843

^bTexas A&M Health Science Center, Department of Molecular and Cellular Medicine, 142 Reynolds Medical Building, College Station, Texas 77843

Abstract. Multicomponent tissue models are viable tools to better understand cell responses in complex environments, but present challenges when investigated with live cell microscopy noninvasively. In this study, integrated nonlinear optical microscopy–optical coherence microscopy (NLOM-OCM) was used to characterize cell interactions within three-dimensional (3-D), multicomponent extracellular matrices. In fibrin–collagen mixtures, 3T3 fibroblasts were observed to recruit both fibrin and collagen fibers while remodeling matrices. Also, NLOM-OCM was used to observe collagen deposition by neonatal human dermal fibroblasts within originally fibrin matrices over an extended time. It was observed that preferentially aligned collagen deposition could be achieved with aligned fibroblasts but that cell alignment could be achieved without aligning the extant extracellular matrix. In summary, this multimodel imaging system has potential for both real-time and longitudinal imaging of living 3-D cultures, which is particularly important for evaluating cell microenvironments in composite scaffolds or serial characterization of engineered tissue constructs during culture. © The Authors. Published by SPIE under a Creative Commons Attribution 3.0 Unported License. Distribution or reproduction of this work in whole or in part requires full attribution of the original publication, including its DOI. [DOI: [10.1117/1.JBO.19.3.036014](https://doi.org/10.1117/1.JBO.19.3.036014)]

Keywords: engineered tissue; nonlinear optical microscopy; optical coherence microscopy.

Paper 130751RR received Oct. 20, 2013; revised manuscript received Jan. 3, 2014; accepted for publication Jan. 8, 2014; published online Mar. 19, 2014.

1 Introduction

Understanding interactions between cells and the extracellular matrix (ECM) has progressed with the development and use of three-dimensional (3-D) tissue models.¹ Four of the most commonly used (natural) 3-D matrices are collagen type I gels,^{2–7} cell-derived matrix,^{8,9} fibrin gels,^{10,11} and basement membrane extract.¹² Fibrin gels, in particular, have exhibited promising properties for tissue engineering applications, including better mechanical properties and stimulation of more collagen and elastic fiber synthesis and deposition when compared to collagen matrices.^{13–17} Generally, these studies have focused on a single specific 3-D model and, when possible, a reconstituted matrix with the simplest necessary component, thereby enabling dissection of matrix protein functions. Also, current microscopy technology has demonstrated the capability to characterize cell–matrix interactions in these 3-D environments over a time course. However, tissues in living organisms can vary substantially in matrix composition and present resident cells with multiple matrix proteins, which may have synergistic and/or competing/antagonistic functions. Thus, multicomponent models are used to characterize cell interactions in tissue environments that more closely resemble *in vivo* conditions. Yet, additional matrix components challenge microscopy techniques in segmenting and delineating cell responses noninvasively and nondestructively throughout an experimental protocol. Here, we report the development and use of integrated nonlinear optical microscopy–

optical coherence microscopy (NLOM-OCM) based on ultrashort optical pulses for the characterization and delineation of fibroblast-mediated 3-D tissue remodeling and matrix deposition in a multicomponent system composed of fibrin and collagen.

Optical methods have shown great promise for nondestructively characterizing parameters of 3-D matrices, including microstructural organization, porosity/pore size, and local matrix remodeling, and cell responses to these parameters, including migration and morphology. Laser scanning confocal reflectance microscopy^{10,18–20} is among the most common techniques to monitor microenvironments without staining or fixing, although it cannot be readily used at depths in excess of 150 μm . OCM^{21,22} is a related technique that uses low-coherence interferometry in addition to a confocal pinhole to filter backscattered light, with an advantage in imaging depth. Unfortunately, the inability of these techniques to distinguish among constituents such as fibrin and collagen complicates characterization of tissue microstructure within a composite matrix and the interpretation of microscopic events in complex systems, such as deposition of new collagen matrix within an existing fibrin network.²³

Two-photon excited fluorescence (TPF),²⁴ second harmonic generation (SHG),^{25,26} and stimulated Raman signal^{27,28} have been used to image thin sections within thick, living biological tissues nondestructively. These nonlinear optical signals are specific to biological molecules and their chemical environments. NLOM is particularly sensitive and well-suited for detecting the ECM, especially fibrillar collagens and mature elastin, without the use of exogenous labels.^{29,30} Tan et al.³¹ combined NLOM with OCM and demonstrated its capability

*Address all correspondence to: Alvin T. Yeh, E-mail: ayeh@tamu.edu

in interrogating the spatiotemporal relationships of structure and function of cells in 3-D culture environments and in response to mechanical stimuli. Herein, we exploited the ability of integrated NLOM-OCM utilizing sub-10-fs pulses to characterize interactions between cells and ECM in engineered constructs, including murine embryonic fibroblast cell line (NIH 3T3) fibroblast seeded reconstituted collagen-fibrin mixtures and fibrin matrices seeded with neonatal human dermal fibroblasts in which new fibrillar collagen was synthesized during culture. Without the use of exogenous agents, both OCM and NLOM rely on spatial inhomogeneities in tissues to provide image contrast. OCM maps the local linear tissue optical scattering properties, and NLOM relies on differences in the local nonlinear optical properties of tissue. These complementary contrast mechanisms enabled label-free imaging of fibrin, in which nonlinear optical signals have not been observed, and collagen using endogenous signals. Thus, we used NLOM-OCM to characterize and delineate remodeling of intertwined collagen and fibrin fibers by seeded fibroblasts. In 3-D fibrin matrices, we used NLOM-OCM to image and characterize deposited collagen anisotropy by embedded fibroblasts over time, cultured under different boundary conditions. Thus, we demonstrated how NLOM-OCM may be used to characterize cell-matrix interactions in complex tissue systems over a time course using endogenous contrast.

2 Methods and Materials

2.1 Experimental System

Our custom NLOM-OCM system has been described previously.³² Briefly, a titanium:sapphire oscillator generating sub-10-fs pulses with central wavelength at 800 nm and 130 nm full-width-at-half-maximum (Femtsource, Femtolasers) was used as a common source for both NLOM and OCM. The integrated NLOM-OCM system utilized a Michelson interferometer configuration where one arm was directed to the tissue construct for both NLOM and sample arm of OCM and the other was used as the reference arm for OCM. NLOM signals generated from the sample were directed to a two-channel detector for image rendering at two different wavelengths for SHG in collagen and TPF in cells. Appropriate long-pass dichroic mirrors and band-pass filters were used to segment SHG (405/20 band-pass filter) and TPF. For TPF, 480/20 and 510/20 band-pass filters were used to image cellular autofluorescence and green fluorescent protein (GFP) fluorescence, respectively. Backscattered laser light from the sample was combined with the return beam of the reference arm and directed to a custom spectrometer for Fourier-domain OCM. Integration of NLOM and OCM enabled microscopic tissue characterization using simultaneously acquired imaging signals that were both constituent specific (nonlinear optical signals) and nonspecific (backscattered laser light). Two-dimensional ($x-y$ plane) images (256×256 pixels) were acquired from various depths (z) at a rate of one frame per 30 s and the average laser power entering the microscope was approximately $P = 60$ mW. A $40\times$ water-immersion microscope objective with 0.75 numerical aperture was used for simultaneous and coregistered NLOM-OCM.

2.2 Cell and Tissue Preparation

Neonatal human dermal fibroblasts (NHDF) and 3T3 fibroblasts (both from ATCC, Manassas, Virginia) were used in our

investigation. NHDF were transfected with recombinant lentiviruses expressing enhanced GFP³³ and selected with $1 \mu\text{g}/\text{ml}$ blasticidin for two weeks prior to initiating experiments. Expression of GFP enabled TPF imaging of cell bodies, especially at depth in light scattering tissue constructs. Cells were cultured in Dulbecco's modified Eagle's medium (DMEM, Invitrogen, Grand Island, New York), containing 10% bovine serum and 1% antibiotic-antimycotic solution (Sigma, St. Louis, Missouri). Cells were cultured near confluency and harvested for experiments from passages 5 to 12. NHDF were seeded in fibrin matrices, and 3T3 fibroblasts were seeded in collagen-fibrin matrices.

2.2.1 NHDF seeded fibrin matrices

NHDF seeded fibrin matrices were initially composed of fibrin and cells at densities of 5 mg/ml and $2 \times 10^6/\text{ml}$, respectively. Fibrin stock solution was formed with bovine fibrinogen (Sigma) dissolved and supplemented with 1 mg/ml of ϵ -amino caproic acid (ϵ -ACA; Sigma), an inhibitor of plasmin activity (which degrades fibrin).^{17,23} This fibrinogen solution was filtered and mixed with 5% fetal bovine serum (FBS) and thrombin (25 U/ml; Sigma) at a ratio of 1:0.02:0.002. Fibrin solution was poured into a cruciform-shaped silicone rubber mold (end-to-end length and arm width of 73 and 20 mm, respectively) placed in a glass Petri dish. Customized bars of porous polyethylene (Small Parts, Miramar, Florida) were positioned at each end of the four arms of the cruciform mold before adding solution. Solution was left undisturbed for 60 min in a humidified CO_2 incubator at 37°C before the mold was removed and the gel was coupled to the biaxial tissue culture device.²⁹ Cruciform-shaped fibrin tissue constructs were clamped within the device via embedded porous polyethylene bars at each end of the four arms. Three stretch ratios were applied to the tissue constructs as shown in Fig. 1, anchored at 1.0:1.0 stretch [Fig. 1(a)], strip biaxial at 1.0:1.1 stretch [Fig. 1(b)], and equibiaxial at 1.1:1.1 stretch [Fig. 1(c)]. The central regions of the samples were longitudinally characterized by NLOM-OCM over three weeks. The culture devices were placed in a humidified CO_2 incubator at 37°C except during imaging. Medium supplemented with 10% FBS, and L-ascorbate, TGF- β Becton Dickinson (BD) was used to support collagen synthesis.^{16,17}

2.2.2 3T3 fibroblasts seeded collagen-fibrin mixture matrices

Collagen-fibrin mixture matrices were formed from stock collagen and fibrin solutions at 1:9 ratio and mixed thoroughly with a suspension of 3T3 fibroblasts. The final densities of collagen, fibrin, and cells were 0.5 mg/ml, 4.5 mg/ml, and $0.5 \times 10^6/\text{ml}$, respectively. Collagen stock (3.5 mg/ml) was composed of rat-tail type I collagen (BD Biosciences, San Jose, California), $5\times$ DMEM, reconstitution buffer, and neutralized with 1 M NaOH.²⁸ One milliliter of mixture solution was added per well of Falcon 12-well plate (Becton Dickinson, San Jose, California) and transferred to a humidified CO_2 incubator at 37°C .

2.3 Image Acquisition

3T3 fibroblast seeded collagen-fibrin mixture matrices were imaged at three time points, 1, 12, and 24 h in culture. At each time point, fibroblast seeded collagen-fibrin matrix was removed from the incubator and placed on the NLOM-OCM

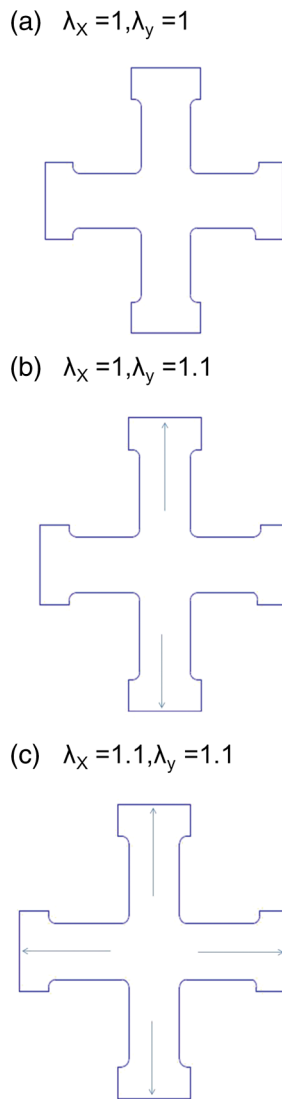


Fig. 1 Cruciform-shaped fibroblast seeded fibrin matrices were cultured under three static stretch conditions, anchored at 1.0:1.0 (a), strip biaxial at 1.0:1.1 (b), and equibiaxial at 1.1:1.1 (c), where λ is the global stretch ratio. Images were acquired from the central region of the cruciform gel.

stage. Images were acquired at a depth of 100 μm below the surface. Coordinates on the mechanical stage were used to recover and image the same cells at each time point. Following image acquisition, culture media were changed and matrices were placed back into incubator until the next imaging session. Image acquisition was completed in ~ 2 min, and the entire sequence of imaging, media replacement, and return to incubator was completed in 3 to 5 min.

Cruciform-shaped NHDF seeded fibrin matrices were cultured in a biaxial bioreactor and imaged within its central region on days 1, 3, 10, and 17. Custom polycarbonate lid fitted with a window assembly with coverslip bottom was used for in-culture microscopic imaging without compromising sterility.³⁴ The position of the glass tube with coverslip bottom was adjusted to contact the tissue construct during microscopic imaging. The lid was sealed with a silicone rubber gasket and secured on top of the culture chamber by screws under aseptic conditions in a class II biosafety cabinet.

2.4 Image Processing and Analysis for Collagen Deposition in Fibrin Matrices Seeded with NHDF

Three NLOM-OCM image stacks were acquired from the central region of each cruciform-shaped, NHDF seeded fibrin matrix. Matrix fiber orientation distribution was analyzed by a MATLAB[®] routine based on a fast Fourier transform algorithm, which has been described previously.²⁹ Collagen fiber segmentation was performed in detection using 405/20 band-pass filter for SHG (see Sec. 2.1). Fibers in OCM not overlapping with SHG were assumed to be fibrin. An alignment index (AI) was used to quantify distributions of collagen and fibrin fiber orientations and to enable statistical comparisons among different culture conditions, that is, the fraction of collagen fibers lying within 20 deg of the predominant direction normalized by that of a random distribution (=0.22). Possible values of AI ranged from 4.55 for strong alignment (i.e., parallel fibers) to 1.00 for random alignment.

3 Results

An advantage of integrating OCM with NLOM is the capability of rendering optically sectioned images without relying solely on nonlinear optical signals. This capability is useful in tissue systems, such as reconstituted fibrin matrices, in which nonlinear optical signals TPF and SHG are not readily observable (e.g., see Figs. 2 to 4). OCM images of unlabeled fibrin gels are shown in Fig. 5 at concentrations of 5 mg/ml [Fig. 5(a)], 7.5 mg/ml [Fig. 5(b)], 10 mg/ml [Fig. 5(c)], and 15 mg/ml [Fig. 5(d)]. The OCM images showed that fibrin porosity decreased with increasing concentration as indicated by decreasing area of void regions between fibrin fibers. Fibrin fibers appeared as straight, rod-like structures, particularly at low concentrations (<10 mg/ml). At high fibrin concentrations, straight, rod-like structures were not as evident, possibly due to aggregation, giving way to a more bulbous morphology, cf., Fig. 5(d).

Fibrin fiber imaging with OCM is nonspecific. Thus, if collagen was mixed into the fibrin gel, imaging signals from OCM could not be easily processed to differentiate between the two matrix proteins. However, SHG in collagen is readily observable, constituent specific, and may be used to segment it from fibrin. Serial images acquired by integrated NLOM-OCM, in which NLOM and OCM images were simultaneously acquired, are shown in Fig. 2 of NIH 3T3 cell seeded fibrin-collagen mixture matrix at a depth of 100 μm below the surface. Total protein concentration was 5 mg/ml with 9:1 ratio of fibrin:collagen, i.e., 4.5:0.5 mg/ml. NLOM-OCM images from two representative regions are shown at three time points (1, 12, 24 h) containing two 3T3 cells (upper images) and from an acellular region (lower images). TPF from the two regions are shown for the three time points in Fig. 2(a). Cellular autofluorescence indicated two cells within the field of view that extended processes over 24 h [Fig. 2(a), upper images]. No TPF was detected from the acellular region [Fig. 2(a), lower images]. Also, notably absent was collagen autofluorescence, which originates from covalent cross-linking and is generally weak from reconstituted collagen³³ [Fig. 2(a)]. Images rendered using SHG are shown in Fig. 2(b), which identified a subset of collagen fibers within the composite matrix. In both cellular (upper images) and acellular regions (lower images), an increase in collagen density was observed, though the increase in collagen density was more pronounced in the cellular region. Nonspecific OCM images simultaneously acquired with

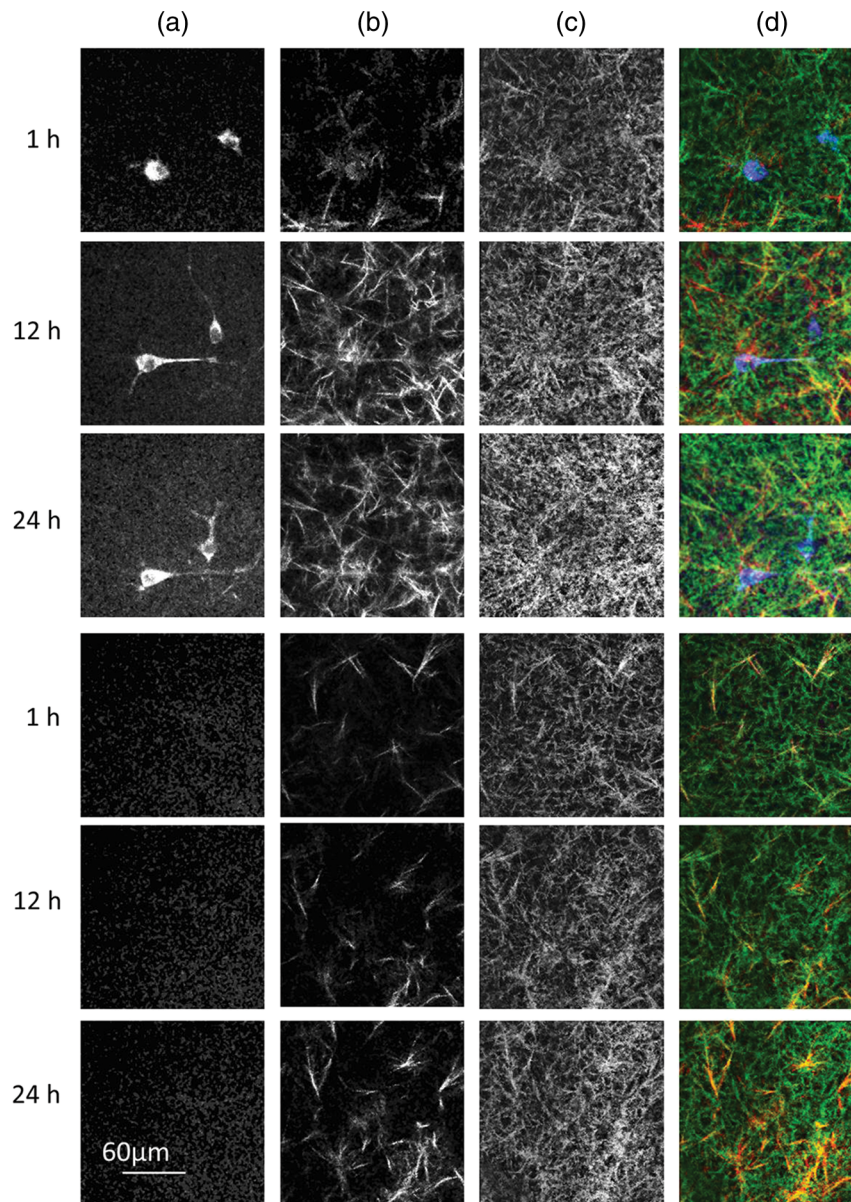


Fig. 2 Longitudinal NLOM-OCM images from cell populated (top) and acellular regions (bottom) of a fibroblast seeded collagen-fibrin matrix. Images rendered by cell-specific two-photon excited autofluorescence (a), second harmonic generation in collagen (b), and nonspecific OCM (c) are overlaid in false color (d) showing relative spatiotemporal distributions of cells (blue), collagen (red), and fibrin (green). NLOM-OCM images were acquired from $\sim 100 \mu\text{m}$ below the surface.

NLOM (TPF and SHG) are shown in Fig. 2(c). OCM images rendered from backscattered laser light revealed a predominantly fibrous morphology. NLOM-OCM images were overlaid and are shown in Fig. 2(d) with cellular TPF, collagen SHG, and OCM false colored blue, red, and green, respectively. In this simple three component tissue construct, OCM structures not overlapping with NLOM (TPF and SHG) were assumed to be fibrin and, thus, green in Fig. 2(d). The overlaid images in Fig. 2(d) revealed dynamic relative spatial distributions of 3T3 cells, collagen, and fibrin that occurred in remodeling of the tissue.

With the ability to segment collagen (and cells) from fibrin fibers in composite matrices, NLOM-OCM was used to image collagen deposition and matrix remodeling in fibroblast seeded fibrin gels. For this study, NHDF were used instead of NIH 3T3

cells because of their comparatively robust translation of collagen protein. Also, NHDF were transfected with GFP to aid in imaging of cell morphology, especially at increased depths. NHDF seeded cruciform-shaped fibrin gels (5 mg/ml) were cultured under three different mechanical boundary conditions, anchored at 1.0:1.0, strip biaxial at 1.0:1.1, and equibiaxial at 1.1:1.1 stretch ratios (see Fig. 1). NLOM-OCM images of fibrin gels were acquired during 17 days of culture from the central region of the cruciform-shaped gel and analyzed to quantify fibrin and collagen fiber orientation distributions. Representative NLOM-OCM images of anchored (1.0:1.0) fibrin gels are shown in Fig. 3 from days 1, 3, 10, and 17. TPF images in Fig. 3(a) showed NHDF initially rounded (day 1) that by day 3 elongated and extended processes, and the number of cells gradually increased in the field of view coinciding with

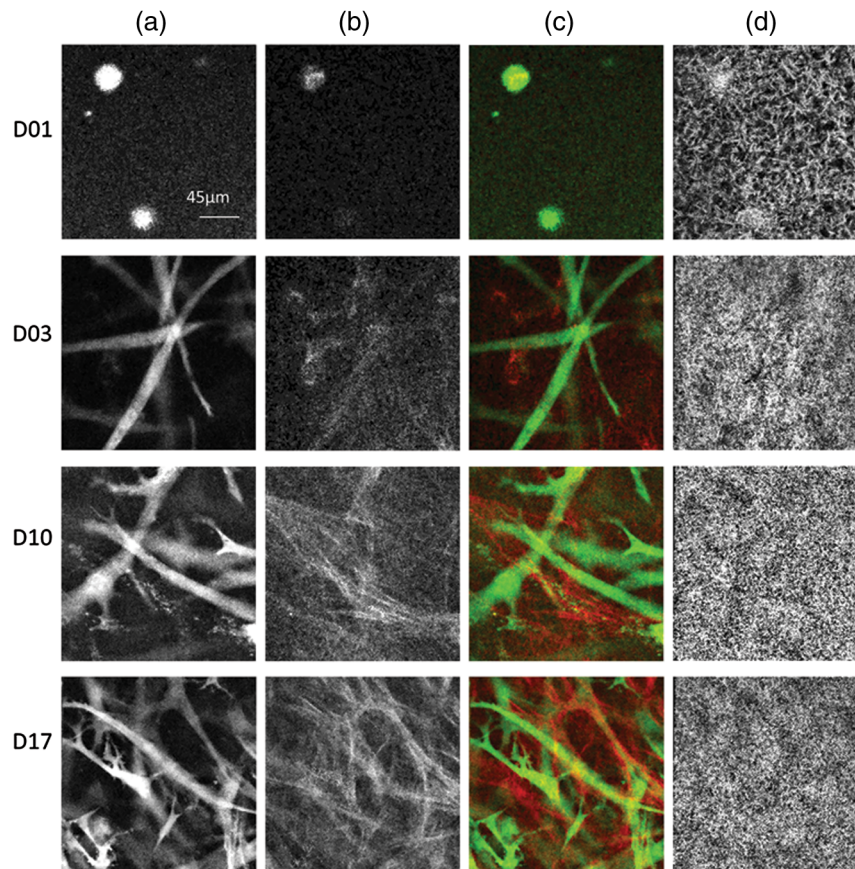


Fig. 3 Representative NLOM-OCM images of fibroblast seeded fibrin matrix anchored at static 1.0:1.0 stretch ratio during 17-day culture. Cellular GFP fluorescence by TPF (a). SHG in collagen (b). Overlay of TPF and SHG, false colored green and red, showing fibroblasts and collagen, respectively (c). Nonspecific OCM images showing dense fibrin matrix (d).

an increase in cell density. Images rendered from SHG and shown in Fig. 3(b) suggested NHDF deposition of collagen that accumulated over time. Due to strong fluorescence signal from cells transfected with GFP, weak TPF was also detected in the SHG channel, especially at early times with rounded cells and before collagen deposition because of autoscaling of the images. This apparent cross-talk decreased with culture time, especially with the deposition of collagen and concurrent increase in SHG signal. Overlay images of TPF and SHG are shown in Fig. 3(c), which are false colored green and red, respectively. The overlay images showed the relative distribution of NHDF and deposited collagen, much of which appeared to align with cell bodies. OCM images are shown in Fig. 3(d). Fibrin fiber and NHDF morphology were distinct on day 1, but at later times, the fibrin gel compacted such that OCM image was dominated by light scattering from the dense fibrin matrix. We note that NLOM-OCM images from NHDF seeded fibrin gels cultured under equibiaxial stretch exhibited qualitatively similar results (data not shown). Both experiments were analyzed for matrix fiber orientation distributions.

An important parameter in engineering tissues is the (an)isotropy or predominant angle and distribution of deposited matrix. Results from anchored fibrin gels suggested that NHDF deposit collagen parallel with its cell body; thus, by controlling cell alignment, it may be possible to control alignment of deposited matrix. To test this hypothesis, NHDF seeded fibrin gels were

cultured under strip biaxial stretch (1.0:1.1 stretch ratio). Representative NLOM-OCM images from the central region are shown in Fig. 4 from 17 days in culture; the principal stretch axis is oriented vertically in the images. TPF images are shown in Fig. 4(a), and consistent with anchored fibrin gels, NHDF morphology was initially rounded on day 1 and elongated and extended processes by day 3. Of note was that elongated cells appeared to preferentially align with principal stretch. SHG images are shown in Fig. 4(b) and indicated an accumulation of collagen with culture time. Collagen within the SHG images appeared to preferentially align with cells in the direction of principal stretch. Overlay images of TPF and SHG images are shown in Fig. 4(c), false colored green and red, respectively. Consistent with anchored fibrin gels, collagen deposition appeared to align with cell bodies, which, when cultured under strip biaxial stretch conditions, preferentially aligned with principal stretch. OCM images are shown in Fig. 4(d), in which, similar to anchored fibrin gels, light scattering was dominated by the dense fibrin matrix. (Over the course of 24 h, NHDF seeded fibrin gels thinned from ~ 1 to ~ 0.1 mm, regardless of culture boundary conditions.)

NLOM-OCM images from three stacks acquired from the central region of NHDF seeded fibrin gels were analyzed to quantify matrix fiber orientation over 17 days of culture (see Materials and Methods), and the results are shown in Fig. 6. Matrix fiber angle distributions are shown for anchored gels

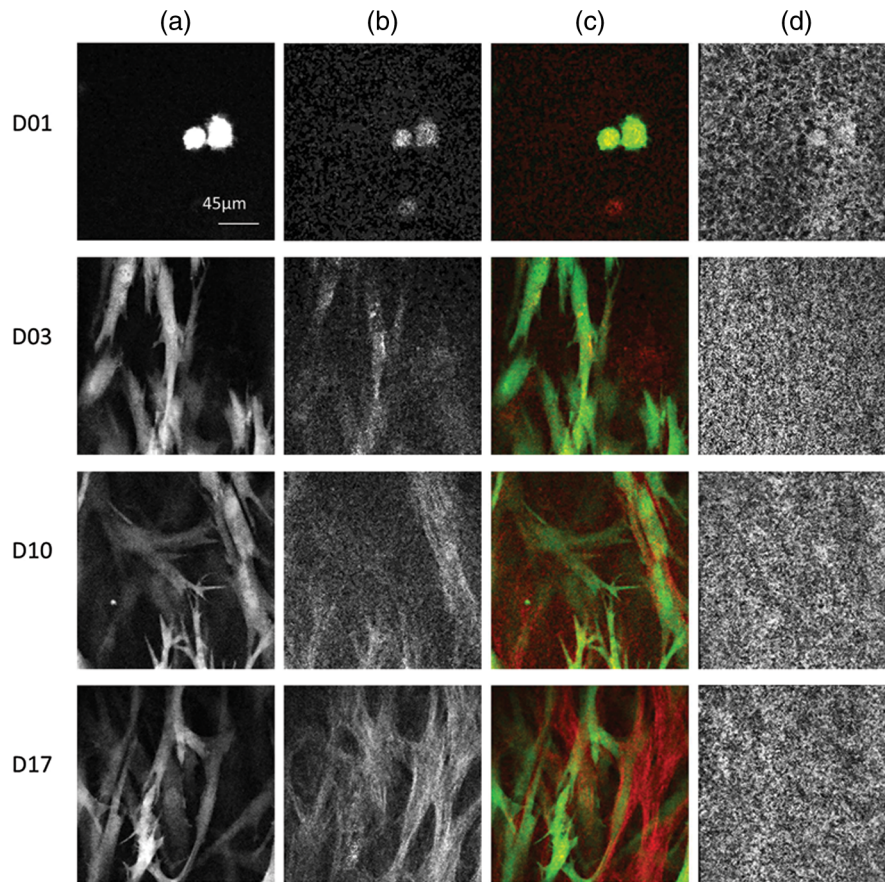


Fig. 4 Representative NLOM-OCM images of fibroblast seeded fibrin matrix cultured for 17 days under static strip biaxial stretch at 1.0:1.1 stretch ratio. Cellular GFP fluorescence by TPF (a). SHG in collagen (b). Overlay of TPF and SHG, false colored green and red, showing fibroblasts and collagen, respectively (c). Nonspecific OCM images showing dense fibrin matrix (d).

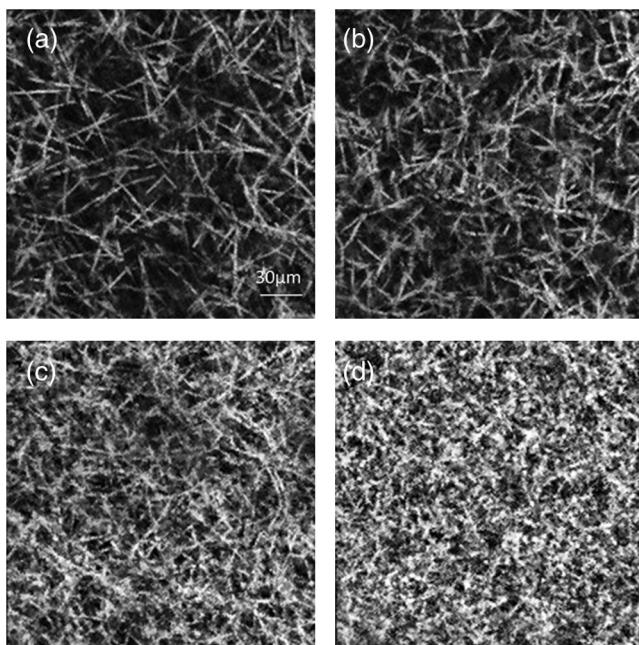


Fig. 5 Representative optical coherence microscopy (OCM) images of 5 mg/ml (a), 7.5 mg/ml (b), 10 mg/ml (c), and 15 mg/ml acellular fibrin matrices (d). Porosity, as indicated by void regions in images, decreased with increasing fibrin concentration.

in Fig. 6(a). For day 1, OCM images were used to calculate fibrin fiber orientation distribution. Fibrin fibers exhibited an isotropic orientation distribution that was also reflected in its calculated alignment index, $AI = 1.0948$. For later time points on days 3, 10, and 17, SHG images were analyzed to calculate deposited collagen fiber orientation distribution; analysis of OCM images for these time points exhibited isotropic fibrin fiber angle distributions (data not shown). In anchored gels, no preferential alignment was exhibited. Consistent with these results for anchored gels, analysis of fibrin and collagen fiber angles in equibiaxially stretched gels also exhibited isotropic distributions. These isotropic distributions are shown in Fig. 6(b), with $AI = 1.1068$ for fibrin fibers on day 1 and 1.1743, 1.1557, and 1.2381 for deposited collagen fibers on days 3, 10, and 17, respectively.

Analysis of matrix fiber angle distributions of strip biaxially stretch gels is shown in Fig. 6(c). Despite a principal stretch of 10%, fibrin fiber angles exhibited isotropic distribution with an $AI = 1.1227$. Yet, this principal stretch was enough to induce NHDF alignment and consequent anisotropic collagen deposition as early as day 3 as evidenced by collagen fiber angle distribution with $AI = 1.2955$ (predominant angle at 0 deg coincident with principal stretch axis). The collagen fiber angle distribution sharpened with culture time along the principal stretch axis with increasing AI , 1.5512 and 1.7261 on days 10 and 17, respectively. It should be noted that fibrin fiber angles

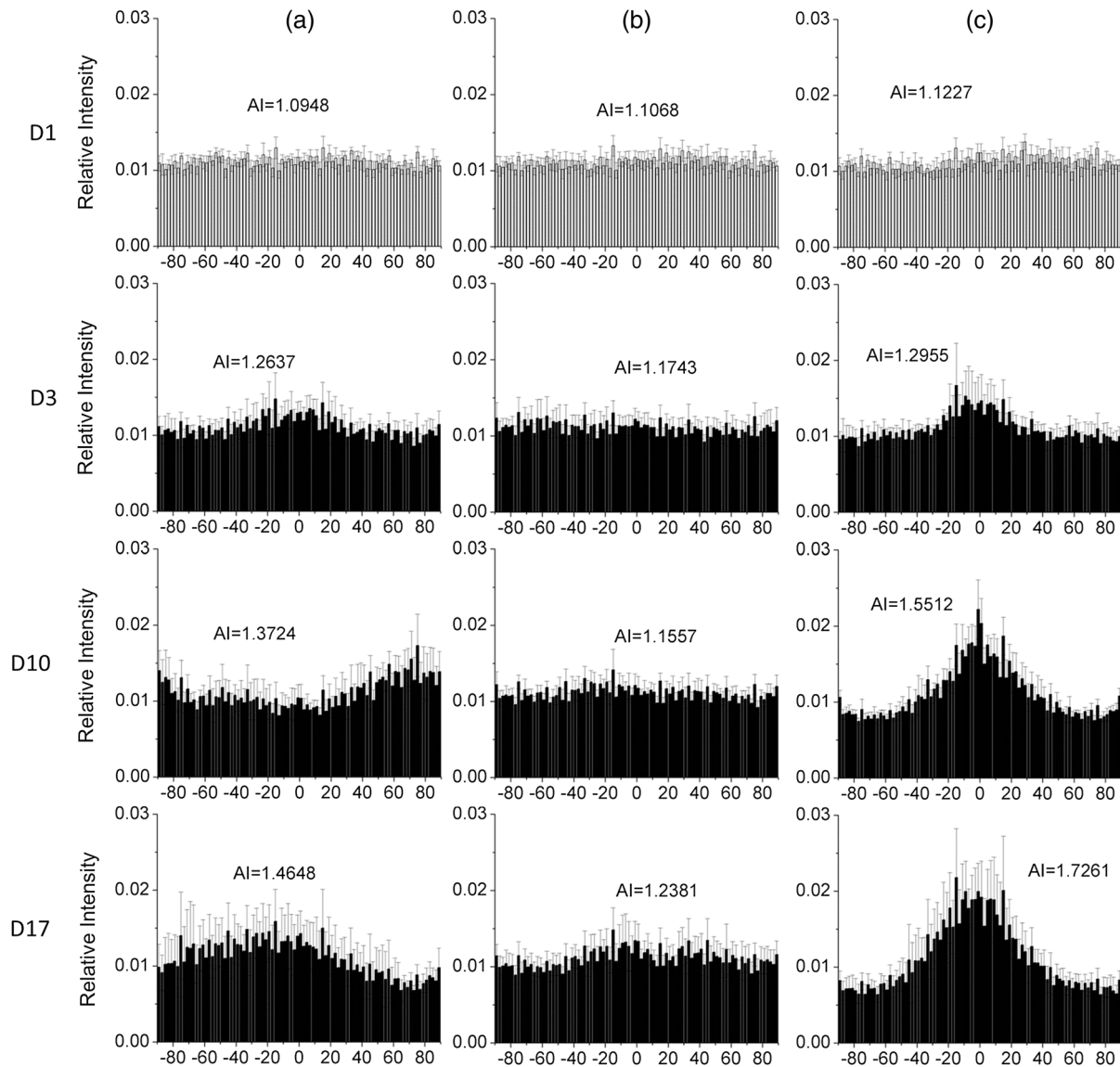


Fig. 6 Fiber orientation distribution analyses of initial fibrin matrix on day 1 and deposited collagen on days 3, 10, and 17 from three-dimensional cultures anchored at 1.0:1.0 stretch ratio (a), equibiaxial 1.1:1.1 stretch (b), and strip biaxial at 1.0:1.1 stretch ratio (c). Relative intensity represents fraction of total fibrin or collagen fibers at orientation angle. Error bars are standard errors ($n = 60$ images for each plot).

exhibited isotropic distributions for each of the days (data not shown).

4 Discussion

An integrated NLOM-OCM system based on sub-10-fs pulses was used to characterize dynamic matrix remodeling and collagen deposition within cell seeded (mixed collagen-fibrin and fibrin) matrices. An advantage of the near-infrared wavelength source used for NLOM-OCM was its ability to image deep into turbid, biological tissues, especially when compared with visible sources used for laser scanning confocal microscopy.³⁴ Use of the common ultrashort pulse laser source helped facilitate simultaneous acquisition and coregistration of NLOM and OCM images. Inherently short coherence length and high peak power of sub-10-fs pulses helped ensure colocalization of imaging signals to the microscopy focus. However, depth of imaging into turbid biological tissue differs for NLOM and OCM

primarily because of different signal wavelengths—higher scattering of upconverted NLOM signals (SHG and TPF) than near-infrared OCM signal. Nevertheless, previous implementations of integrated NLOM-OCM have recognized the advantages of combining techniques with complementary contrast mechanisms.^{31,35,36} Here, these complementary techniques were used to noninvasively image multicomponent tissue constituents, a subset of which had observable endogenous NLOM (TPF and SHG) signals. In these tissue systems, OCM provided context to the images of constituents with nonlinear contrast, i.e., global view of tissue microenvironment morphology, albeit without inherent chemical specificity.

In a multicomponent tissue system of 3T3 cell seeded fibrin-collagen matrix (see Fig. 2), NLOM-OCM was used to image matrix remodeling over a time course of 24 h. Over this 24-h time course, 3T3 cells were captured extending their processes by TPF (autofluorescence). Simultaneously acquired SHG and

OCM images suggested that cells actively controlled their local environment by remodeling the composite matrix, particularly recruitment of collagen and fibrin fibers. Matrix remodeling and recruitment were evidenced in the stellate arrangement of collagen and fibrin fibers emanating from cell bodies and in the increase in fiber density over time. This increase in matrix density was observed both near and far from 3T3 cells because of (cell traction mediated) gel contraction, albeit more pronounced in the vicinity of cells. For collagen in particular, we do not believe its increase in density was due to 3T3 synthesis and deposition for two reasons. The media was not supplemented for protein synthesis, e.g., ascorbic acid (vitamin c), and even in synthetic media, 3T3 cells were poor in depositing collagen matrix. This was the primary reason in our choice of NHDF in experiments imaging collagen deposition within cell seeded fibrin matrices (cf., Figs. 3, 4, 6).

Biomaterials impart cues that play a critical role in the success of tissue engineering approaches. Given that few biomaterials possess all the necessary characteristics to promote the desired cellular and tissue behavior, hybrid or composite biomaterials have been developed to deliver the beneficial properties of multiple materials into a superior matrix. Rowe and Stegemann³⁷ showed that collagen-fibrin composites may be used to tailor material properties of the construct, and selected protein combinations showed improved function and mechanical behavior. Berglund et al.³⁸ presented a method to incorporate organized, intact elastin into collagen-based tissue engineered blood vessels to form hybrid constructs that better mimicked arterial physiology and exhibited improved mechanical properties. Here, NLOM-OCM provided longitudinal, constituent specific images in composite matrices through a time course (see Fig. 2). Cell morphology and collagen and fibrin fiber organization were visualized simultaneously and delineated in a viable or live cell state. Long-term (>24 h) live cell experiments may be accommodated by adapting this imaging setup with bioreactors or chambers^{39,40} such that parameters including temperature, humidity, and carbon dioxide level may be controlled. In such configurations, live cell NLOM-OCM may be used to probe microscopic events underlying long-term processes, including tissue morphogenesis, growth, and healing.

Central to the processes of tissue morphogenesis, growth, and healing is the deposition of matrix proteins with proper 3-D organization for tissue function. With the aid of a custom biaxial bioreactor, NLOM-OCM was used to image collagen deposition within NHDF seeded, cruciform-shaped fibrin matrices cultured under three mechanical environments, anchored (1.0:1.0 stretch ratio), equibiaxial (1.1:1.1), and strip biaxial (1.0:1.1). NLOM-OCM images were acquired from the central region of the cruciform-shaped gel over 17 days.³⁴ Sterility was maintained by performing live cell microscopy through a custom coverslip window. Similar to observations of 3T3 cells in fibrin-collagen mixed matrices, as early as day 1, NHDF seeded in fibrin matrices cultured under all conditions were observed to remodel the initially fibrin matrix even though cell morphology was round. Fibrin fiber density increased with time, particularly in the first 24 h, because of dramatic gel compaction indicated by thinning from ~ 1 to ~ 0.1 mm. For anchored and equibiaxially stretched fibrin matrices, orientation of deposited collagen fibers was isotropically distributed reflecting the orientation of NHDF, which was not surprising given the culture conditions. The density of collagen was observed to increase over the 17-day period.

Strip biaxial stretch culture condition was imposed on the cruciform-shaped gel to break its planar symmetry and induce alignment of NHDF (and, thus, collagen deposition) along direction of principal stretch. NLOM-OCM images over the 17-day period indicated NHDF as well as collagen deposition preferentially aligned with principal stretch (see Fig. 4). Thus, anisotropic matrix deposition may be accomplished by inducing preferential alignment of resident cells. However, the mechanism of cell alignment remains to be defined. In our system, preferential cell alignment was accomplished without inducing an anisotropic distribution of fibrin fiber angles and, therefore, was not driven by contact guidance (see Fig. 6). Principal stress was aligned with principal stretch and, therefore, may have increased stiffness of coincident fibrin fibers. Increased stiffness may occur if the constituents exhibit nonlinear mechanical responses, i.e., material stiffens with increased stretch. However for fibrin matrices, it reportedly exhibits linear elasticity, which would not mechanically behave in this manner.

For many tissues, including skin, ligaments, and arteries, the most important load-bearing component of the tissue is collagen. However, its arrangement or alignment pattern rather than the mere presence of collagen controls the tissue's mechanical functionality. Several strategies have been employed to produce engineered tissues with a prescribed fiber alignment and ultimately produce functional replacement tissue. These strategies include magnetic forces, gel boundary conditions, substratum topology, and mechanical loading.⁴¹⁻⁴⁴ However, it is less clear how to ensure the development of appropriately oriented cells and collagen fibers. In the current study, this is, to our knowledge, the first visualization of collagen deposition, spatial distribution, and organization within extant fibrin matrix without staining or labeling, demonstrating NLOM-OCM ability to noninvasively and serially assess ECM development. Biaxial bioreactor having both a mechanical testing platform and a stage for NLOM-OCM imaging was designed⁴⁵ and is under development.³⁴ Combined with bioreactors, multimodal imaging will enable future serial measurements on individual constructs over extended time courses to better visualize and understand biological, chemical, mechanical, and materials effects on cellular responses that drive bulk tissue properties.

5 Summary

The ability of NLOM-OCM to visualize different constituents in 3-D extracellular matrices was demonstrated. Engineered tissue constructs were composed of fibrin or collagen-fibrin mixed with cells. This multimodal microscopy system provided different yet complementary information that allowed noninvasive, spatially localized characterization of cell-ECM interactions. Our results suggested that with advances in instrumentation, NLOM-OCM has potential for both real-time and long-term imaging of living, dynamic, 3-D cultures particularly important for the future development of optimal microenvironments for cells in 3-D scaffolds or serial characterization of engineered tissue constructs during culture.

Acknowledgments

This work was supported in part by the National Science Foundation (CBET-1033660 to A.T.Y.).

References

1. E. Cukierman et al., "Taking cell-matrix adhesions to the third dimension," *Science* **294**(5547), 1708–1712 (2001).
2. F. Grinnell, "Fibroblast-collagen-matrix contraction: growth-factor signalling and mechanical loading," *Trends Cell Biol.* **10**(9), 362–365 (2000).
3. S. Rhee and F. Grinnell, "Fibroblast mechanics in 3D collagen matrices," *Adv. Drug Deliv. Rev.* **59**(13), 1299–1305 (2007).
4. V. C. Sandulache et al., "Fetal dermal fibroblasts retain a hyperactive migratory and contractile phenotype under 2- and 3-dimensional constraints compared to normal adult fibroblasts," *Tissue Eng.* **13**(11), 2791–2801 (2007).
5. D. Karamichos, R. A. Brown, and V. Mudda, "Complex dependence of substrate stiffness and serum concentration on cell-force generation," *J. Biomed. Mater. Res. A* **78**(2), 407–415 (2006).
6. K. Maaser et al., "Functional hierarchy of simultaneously expressed adhesion receptors: integrin $\alpha 2 \beta 1$ but not CD44 mediates MV3 melanoma cell migration and matrix reorganization within three-dimensional hyaluronan-containing collagen matrices," *Mol. Biol. Cell* **10**(10), 3067–3079 (1999).
7. F. Grinnell and W. M. Petroll, "Cell motility and mechanics in three-dimensional collagen matrices," *Annu. Rev. Cell Dev. Biol.* **26**(1), 335–361 (2010).
8. K. M. Yamada and E. Cukierman, "Modeling tissue morphogenesis and cancer in 3D," *Cell* **130**(4), 601–610 (2007).
9. E. Cukierman, R. Pankov, and K. M. Yamada, "Cell interactions with three-dimensional matrices," *Curr. Opin. Cell Biol.* **14**(5), 633–640 (2002).
10. A. Hartmann, P. Boukamp, and P. Friedl, "Confocal reflection imaging of 3D fibrin polymers," *Blood Cells Mol. Dis.* **36**(2), 191–193 (2006).
11. T. Sun, J. Haycock, and S. Macneil, "In situ image analysis of interactions between normal human keratinocytes and fibroblasts cultured in three-dimensional fibrin gels," *Biomaterials* **27**(18), 3459–3465 (2006).
12. D. C. Radisky et al., "Rac1b and reactive oxygen species mediate MMP-3-induced EMT and genomic instability," *Nature* **436**(7047), 123–127 (2005).
13. M. Thie et al., "Aortic smooth muscle cells in collagen lattice culture: effects on ultrastructure, proliferation and collagen synthesis," *Eur. J. Cell Biol.* **55**(2), 295–304 (1991).
14. R. A. Clark et al., "Collagen matrices attenuate the collagen-synthetic response of cultured fibroblasts to TGF- β ," *J. Cell Sci.* **108**(3), 1251–1261 (1995).
15. E. D. Rassl, T. R. Oegema, and R. T. Tranquillo, "Fibrin as an alternative biopolymer to type-I collagen for the fabrication of a media equivalent," *J. Biomed. Mater. Res.* **60**(4), 607–612 (2002).
16. M. R. Neidert et al., "Enhanced fibrin remodeling in vitro with TGF- β , insulin and plasmin for improved tissue-equivalents," *Biomaterials* **23**(17), 3717–3731 (2002).
17. J. L. Long and R. T. Tranquillo, "Elastic fiber production in cardiovascular tissue equivalents," *Matrix Biol.* **22**(4), 339–350 (2003).
18. K. M. Hakkinen et al., "Direct comparisons of the morphology, migration, cell adhesions, and actin cytoskeleton of fibroblasts in four different three-dimensional extracellular matrices," *Tissue Eng. Part A* **17**(5), 713–724 (2011).
19. S. L. Voytik-Harbin et al., "Simultaneous mechanical loading and confocal reflection microscopy for three-dimensional microbiomechanical analysis of biomaterials and tissue constructs," *Microsc. Microanal.* **9**(1), 74–85 (2003).
20. K. Wolf et al., "Compensation mechanism in tumor cell migration: mesenchymal-amoeboid transition after blocking pericellular proteolysis," *J. Cell Biol.* **160**(2), 267–277 (2003).
21. J. A. Izatt et al., "Optical coherence microscopy in scattering media," *Opt. Lett.* **19**(8), 590–592 (1994).
22. A. L. Clark et al., "Detection and diagnosis of oral neoplasia with an optical coherence microscope," *J. Biomed. Opt.* **9**(6), 1271–1280 (2004).
23. T. L. Tuan et al., "In vitro fibroplasia: matrix contraction, cell growth, and collagen production of fibroblasts cultured in fibrin gels," *Exp. Cell Res.* **223**(1), 127–134 (1996).
24. W. Denk, J. H. Strickler, and W. W. Webb, "Two-photon laser scanning fluorescence microscopy," *Science* **248**(4951), 73–76 (1990).
25. P. J. Campagnola et al., "Three-dimensional high-resolution second harmonic generation imaging of endogenous structural proteins in biological tissues," *Biophys. J.* **82**(1), 493–508 (2002).
26. Y. Guo et al., "Second-harmonic tomography of tissues," *Opt. Lett.* **22**(17), 1323–1325 (1997).
27. J. Cheng, L. D. Book, and X. S. Xie, "Polarization coherent anti-Stokes Raman scattering microscopy," *Opt. Lett.* **26**(17), 1341–1343 (2001).
28. E. O. Potma et al., "Real-time visualization of intracellular hydrodynamics in single living cells," *Proc. Natl. Acad. Sci. U. S. A.* **98**(4), 1577–1582 (2001).
29. J. Hu, J. D. Humphrey, and A. T. Yeh, "Characterization of engineered tissue development under biaxial stretch using nonlinear optical microscopy," *Tissue Eng. Part A* **15**(7), 1553–1564 (2009).
30. L. E. Niklason et al., "Enabling tools for engineering collagenous tissues integrating bioreactors, intravital imaging, and biomechanical modeling," *Proc. Natl. Acad. Sci. U. S. A.* **107**(8), 3335–3339 (2010).
31. W. Tan et al., "Imaging cellular responses to mechanical stimuli within three-dimensional tissue constructs," *Microsc. Res. Tech.* **70**(4), 361–371 (2007).
32. Q. Wu, B. E. Applegate, and A. T. Yeh, "Cornea microstructure and mechanical responses measured with nonlinear optical and optical coherence microscopy using sub-10-fs pulses," *Biomed. Opt. Express* **2**(5), 1135–1146 (2011).
33. P. F. Lee et al., "Angiogenic responses are enhanced in mechanically and microscopically characterized, microbial transglutaminase crosslinked collagen matrices with increased stiffness," *Acta Biomater.* **9**(7), 7178–7190 (2013).
34. Y. Bai et al., "Sequential multimodal microscopic imaging and biaxial mechanical testing of living multicomponent tissue constructs," (in revision).
35. S. Tang et al., "Combined multiphoton microscopy and optical coherence tomography using a 12-fs broadband source," *J. Biomed. Opt.* **11**(2), 020502 (2006).
36. L. Moreaux et al., "Membrane imaging by simultaneous second-harmonic generation and two-photon microscopy," *Opt. Lett.* **25**(5), 320–322 (2000).
37. S. L. Rowe and J. P. Stegemann, "Interpenetrating collagen-fibrin composite matrices with varying protein contents and ratios," *Biomacromolecules* **7**(2), 2942–2948 (2006).
38. J. D. Berglund, R. M. Nerem, and A. Sambanis, "Incorporation of intact elastin scaffolds in tissueengineered collagen-based vascular grafts," *Tissue Eng.* **10**(1), 1526–1535 (2004).
39. J. W. Young et al., "Measuring single-cell gene expression dynamics in bacteria using fluorescence time-lapse microscopy," *Nat. Protoc.* **7**(7310), 80–88 (2011).
40. M. Baker, "Cellular imaging: taking a long, hard look," *Nature* **466**(4), 1137–1140 (2010).
41. R. T. Tranquillo et al., "Magnetically orientated tissue-equivalent tubes: application to a circumferentially orientated media-equivalent," *Biomaterials* **17**(4), 349–357 (1996).
42. K. D. Costa, E. J. Lee, and J. W. Holmes, "Creating alignment and anisotropy in engineered heart tissue: role of boundary conditions in a model three-dimensional culture system," *Tissue Eng.* **9**(4), 567–577 (2003).
43. J. Glass-Brudzinski, D. Perizzolo, and D. M. Brunette, "Effects of substratum surface topography on the organization of cells and collagen fibers in collagen gel cultures," *J. Biomed. Mater. Res.* **61**(1), 608–618 (2002).
44. V. C. Mudda et al., "Molecular responses of human dermal fibroblasts to dual cues: contact guidance and mechanical load," *Cell Motil. Cytoskeleton* **45**(4), 1–9 (2000).
45. J. D. Humphrey et al., "A theoretically-motivated biaxial tissue culture system with intravital microscopy," *Biomech. Model. Mechanobiol.* **7**, 323–334 (2008).

Yuqiang Bai earned his BS in physics from Shanxi University in 1999 and an MS in optics from Shanghai Jiao Tong University in 2002. He worked in the telecommunications industry for four years and is currently a doctoral candidate in the Tissue Microscopy Lab in the Department of Biomedical Engineering at Texas A&M University where he specializes in integrated nonlinear optical microscopy and optical coherence microscopy instrumentation and its application

to imaging dynamic cell-matrix interactions and remodeling in engineered tissues.

Po-Feng Lee earned his BSc in mechanical engineering from Tatung University in 1999, MSc in mechanical engineering from University of Colorado at Boulder in 2005 and completed his PhD in biomedical engineering from Texas A&M University at College Station in 2012. After graduation, he worked as postdoctoral research associate in Tissue Microscopy Lab in Texas A&M University with his research focusing on angiogenic responses to extracellular matrix properties. He is also an expert in nonlinear and optical coherence microscopy technologies, biomechanics and mechanobiology.

Holly C. Gibbs earned her BS in biomedical engineering from Texas A&M University in 2006 and MSc in genomics and pathways biology from the University of Edinburgh in 2008. Currently, she is a doctoral candidate in the Tissue Microscopy Lab in the Department of Biomedical Engineering at Texas A&M University where she specializes in the application of ultrashort laser technology in the field of

developmental biology, specifically vertebrate brain patterning and development.

Kayla J. Bayless earned her BS in Molecular Biology from Texas Lutheran College in 1994 and completed a PhD in Medical Physiology from Texas A&M University in 1999. Currently, she is an associate professor of Molecular and Cellular Medicine at Texas A&M Health Science Center. Her research focuses on better understanding basic signals that regulate endothelial sprouting and movement in three-dimensional environments.

Alvin T. Yeh earned his BSE in chemical engineering from the University of Michigan in 1993 and completed his PhD in chemistry at the University of California at Berkeley in 2000. Currently, he is associate professor of biomedical engineering at Texas A&M University, where his research focuses on instrumentation development for imaging modalities using ultrashort pulses and their application to study angiogenesis and cell-matrix interactions in engineered tissues and embryonic development.